Weierstraß-Institut
für Angewandte Analysis und Stochastik
Leibniz-Institut im Forschungsverbund Berlin e. V.

Preprint ISSN 2198-5855

Comparison of thermodynamically consistent charge carrier flux discretizations for Fermi–Dirac and Gauss–Fermi statistics

Patricio Farrell[1], Matteo Patriarca[2], Jürgen Fuhrmann[1], Thomas Koprucki[1]

submitted: September 6, 2017

[1] Weierstrass Institute
Mohrenstr. 39
10117 Berlin
Germany
E-Mail: patricio.farrell@wias-berlin.de
juergen.fuhrmann@wias-berlin.de
thomas.koprucki@wias-berlin.de

[2] University of Rome "Tor Vergata"
Via del Politecnico 1
00133 Roma
Italy
E-Mail: matteo.patriarca@uniroma2.it

No. 2424
Berlin 2017

2010 *Mathematics Subject Classification.* 65N08, 35K55.

Key words and phrases. Scharfetter–Gummel schemes, (organic) semiconductors, nonlinear diffusion, thermodynamic consistency, finite volume scheme, Gauss–Fermi integral, Fermi–Dirac integral.

This work received funding via the Research Center Matheon supported by ECMath in project D-CH11 and the DFG CRC 787 "Semiconductor Nanophotonics".

Edited by
Weierstraß-Institut für Angewandte Analysis und Stochastik (WIAS)
Leibniz-Institut im Forschungsverbund Berlin e. V.
Mohrenstraße 39
10117 Berlin
Germany

Fax: +49 30 20372-303
E-Mail: preprint@wias-berlin.de
World Wide Web: http://www.wias-berlin.de/

Comparison of thermodynamically consistent charge carrier flux discretizations for Fermi–Dirac and Gauss–Fermi statistics

Patricio Farrell, Matteo Patriarca, Jürgen Fuhrmann, Thomas Koprucki

Abstract

We compare three thermodynamically consistent Scharfetter–Gummel schemes for different distribution functions for the carrier densities, including the Fermi–Dirac integral of order 1/2 and the Gauss–Fermi integral. The most accurate (but unfortunately also most costly) generalized Scharfetter–Gummel scheme requires the solution of an integral equation. We propose a new method to solve this integral equation numerically based on Gauss quadrature and Newton's method. We discuss the quality of this approximation and plot the resulting currents for Fermi–Dirac and Gauss–Fermi statistics. Finally, by comparing two modified (diffusion-enhanced and inverse activity based) Scharfetter–Gummel schemes with the more accurate generalized scheme, we show that the diffusion-enhanced ansatz leads to considerably lower flux errors, confirming previous results (J. Comp. Phys. 346:497-513, 2017).

1 Introduction

The classical Scharfetter-Gummel scheme in combination with a Voronoï finite volume method provides a discrete approximation to drift-diffusion currents in non-degenerate semiconductors (Boltzmann regime). The scheme is consistent with the thermodynamic equilibrium in the sense that the (full) zero-bias solution coincides with the unique thermodynamic equilibrium. This consistency helps to avoid unphysical steady state dissipation, see [1]. Furthermore, the consistent discretization of dissipative effects is crucial when coupling the semiconductor equations to heat transport models.

However, the classical Scharfetter-Gummel scheme is only consistent when one is justfied in using the Boltzmann approximation. Non-Boltzmann distribution functions describing degenerate semiconductors are required for organic semiconductors, highly doped materials and semiconductor devices operated at cryogenic temperatures as shown e.g. by [8]. Strong degeneracy effects make it mandatory to employ Fermi-Dirac statistics. Therefore, it is crucial to develop generalizations of the Scharfetter-Gummel scheme beyond the Boltzmann approximation. A number of schemes for degenerate semiconductors proposed in the literature [12], [7], [14] are not thermodynamically consistent.

[1], [10], and [5] proposed modified Scharfetter-Gummel schemes which are thermodynamically consistent. Based on [2], [9] introduced (an accurate but costly) thermodynamically consistent generalized Scharfetter-Gummel scheme which requires the solution of an integral equation summarized in Section 4.
[3] analysed these schemes and compared their accuracy in the case of the Blakemore approximation.

The focus of the present paper is on the Fermi-Dirac integral of order 1/2 as well as the Gauss-Fermi integral. Furthermore, in Section 5 we present a new algorithm to solve the integral equation proposed in [9] based on Gauss quadrature and Newton's method. Using this numerical flux as reference, we compare the performance of the two modified Scharfetter-Gummel schemes in Section 6.

DOI 10.20347/WIAS.PREPRINT.2424 Berlin 2017

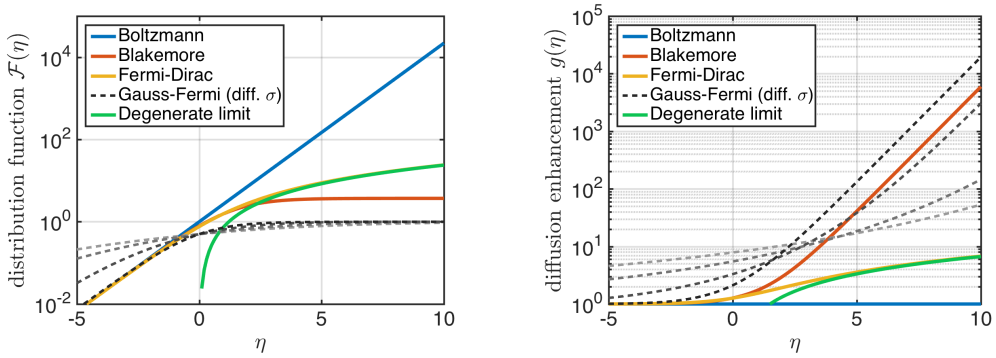

Figure 1: Distribution functions and their corresponding diffusion enhancement (6).

2 Van Roosbroeck system and distribution functions

We consider the stationary van Roosbroeck system of charge transport in semiconductors using standard notation from [3] (ψ: electrostatic potential, φ_n, φ_p: quasi-Fermi potentials, η_n, η_p: chemical potentials):

$$-\nabla\cdot(\varepsilon_0\varepsilon_r\nabla\psi) = q\,(p - n + C)\,, \tag{1a}$$

$$\nabla\cdot\mathbf{j}_n = qR, \qquad \mathbf{j}_n = -q\mu_n n\nabla\varphi_n, \tag{1b}$$

$$\nabla\cdot\mathbf{j}_p = -qR, \qquad \mathbf{j}_p = -q\mu_p p\nabla\varphi_p \tag{1c}$$

where μ_n and μ_p denote the electron and hole mobilities, C the doping, R the recombination rate. The electron and hole densities are defined by

$$n = N_c\mathcal{F}(\eta_n), \qquad \eta_n = \frac{q(\psi-\varphi_n) - E_c}{k_BT}, \tag{2a}$$

$$p = N_v\mathcal{F}(\eta_p), \qquad \eta_p = \frac{q(\varphi_p-\psi) + E_v}{k_BT}. \tag{2b}$$

Distribution functions describe how potentials and charge carriers are related. For inorganic, 3D bulk semiconductors with parabolic bands this relation is given by the Fermi-Dirac integral of order 1/2,

$$\mathcal{F}(\eta) = F_{1/2}(\eta) := \frac{2}{\sqrt{\pi}}\int_0^\infty \frac{\xi^{1/2}}{\exp(\xi-\eta)+1}d\xi, \tag{3}$$

which can be approximated by a Blakemore ($\mathcal{F}(\eta) = (\exp(-\eta)+\gamma)^{-1}$ with $\gamma = 0.27$) or Boltzmann ($\mathcal{F}(\eta) = \exp(\eta)$) distribution in the low density limit. For large arguments, $F_{1/2}(\eta)$ can be approximated by the degenerate limit $\frac{2}{\sqrt{\pi}}\eta^{3/2}$. For organic semiconductors the Gauss-Fermi integral, a term coined by [11],

$$\mathcal{F}(\eta) = \mathcal{G}(\eta;\sigma) := \frac{1}{\sqrt{2\pi}\sigma}\int_{-\infty}^\infty \frac{\exp(-\frac{\xi^2}{2\sigma^2})}{\exp(\xi-\eta)+1}d\xi, \tag{4}$$

describes the relationship between potentials and carrier densities. The variance σ measures the disorder of the energy levels. The Gauss-Fermi integral reduces to a Blakemore distribution function (with $\gamma = 1$) for vanishing disorder σ, corresponding to a δ-shaped density of states, describing a single transport level. All relevant functions are depicted in Figure 1.

In the following we restrict our considerations to the continuity equation for electrons, partially omitting the index n. The electron current can be rewritten in drift-diffusion form,

$$\mathbf{j}_n = -q\mu_n n\nabla\psi + qD_n\nabla n. \tag{5}$$

The diffusion coefficient D_n is linked to the carrier mobilities by a generalized Einstein relation $\frac{D_n}{\mu_n} = \frac{k_BT}{q}g(\eta_n)$, where the *diffusion enhancement* is given by

$$g(\eta) = \frac{\mathcal{F}(\eta)}{\mathcal{F}'(\eta)} = \frac{1}{\big(\log\mathcal{F}(\eta)\big)'}. \tag{6}$$

For the Boltzmann distribution, we have $g \equiv 1$. Therefore, g is a measure of the degeneracy (i. e. the deviation from the Boltzmann regime), see Figure 1.

3 Finite volume discretization and thermodynamic consistency

We partion the domain Ω into control volumes (Voronoï cells) ω_K such that $\Omega = \bigcup_{K=1}^N \omega_K$. With each control volume we associate a node $\mathbf{x}_K \in \omega_K$. Via the divergence theorem we obtain after integration over each control volume a discrete version of the continuity equation (1b). Consistent with the continuous van Roosbroeck system, this *finite volume* discretization describes the change of the carrier density within a control volume. The corresponding numerical flux j describing the flow between neighboring control volumes can be expressed as a function, depending nonlinearly on the values $\psi_K, \psi_L, \eta_K, \eta_L$ such that

$$j(\psi_K, \psi_L, \eta_K, \eta_L) \approx \frac{1}{|\partial\omega_K \cap \partial\omega_L|}\int_{\partial\omega_K\cap\partial\omega_L} \mathbf{j}\cdot\mathbf{n}\, dS.$$

Here a function with subindex, e.g. K, denotes evaluation of the function at the node $\mathbf{x}_K$.
[4] give more details on the derivation of this scheme.

We require our numerical current approximation to satisfy *thermodynamic consistency*, a property which holds at the continuous level: constant quasi Fermi potentials lead to vanishing currents. Thus, setting any discrete numerical flux between two adjacent discretization nodes $\mathbf{x}_K$ and $\mathbf{x}_L$ to zero

$$j = j(\eta_L, \eta_K, \psi_L, \psi_K) = 0$$

shall imply

$$\frac{\psi_L - \psi_K}{U_T} =: \delta\psi_{KL} \stackrel{!}{=} \delta\eta_{KL} := \eta_L - \eta_K \tag{7}$$

where $U_T = k_BT/q$ denotes the thermal voltage.

4 Generalized Scharfetter-Gummel schemes

If one assumes that the (unknown) flux j between two cells is constant, it fulfills the integral equation, studied by [2, 9],

$$\int_{\eta_K}^{\eta_L}\left(\frac{j_n/j_0}{\mathcal{F}(\eta)} + \frac{\psi_L - \psi_K}{U_T}\right)^{-1} d\eta = 1, \quad j_0 = q\mu_n N_c\frac{U_T}{h_{KL}} \tag{8}$$

(a) Fermi-Dirac (b) Gauss-Fermi ($\sigma = 5$)

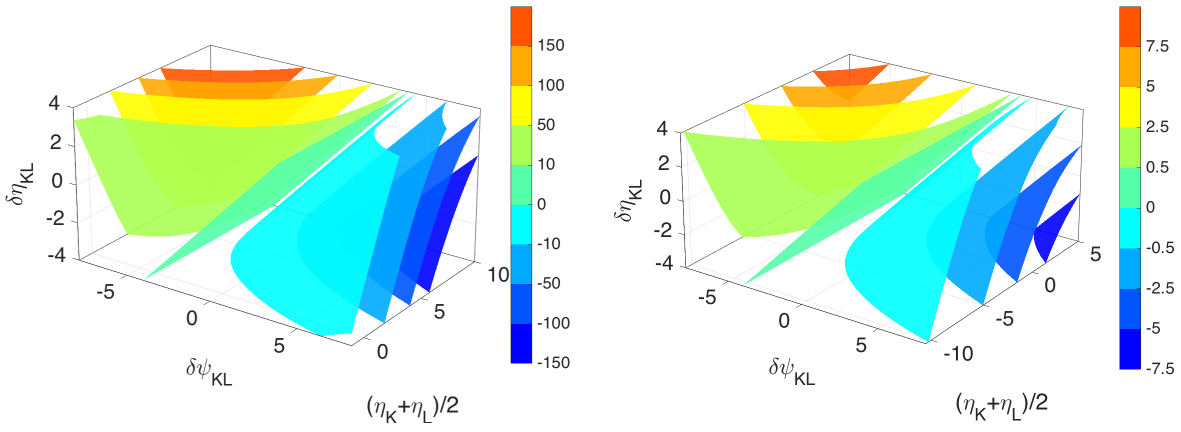

Figure 2: Isosurfaces of the generalized Scharfetter-Gummel flux (8) computed via (11). The plane $\delta\psi_{KL} - \delta\eta_{KL} = 0$ in the middle of both figures corresponds to the thermodynamic consistency (7), where the current vanishes thus separating negative and positive currents.

where the integration limits are given by $\eta_K = \eta_n(\psi_K, \varphi_K)$ and $\eta_L = \eta_n(\psi_L, \varphi_L)$. [6] showed that for strictly monotonously increasing $\mathcal{F}(\eta)$ this equation has always a unique solution. We will refer to it as the *generalized* Scharfetter-Gummel flux.

For the Boltzmann approximation we recover from (8) the classical scheme by [13],

$$j_{\text{sg}} = B(\delta\psi_{KL})\, e^{\eta_L} - B(-\delta\psi_{KL})\, e^{\eta_K}, \tag{9}$$

for the non-dimensionalized edge current $j_{\text{sg}} = j_n/j_0$ and the Bernoulli function $B(x) := x/(e^x - 1)$. [9] showed that the Blakemore approximation $\mathcal{F}(\eta) = \frac{1}{e^{-\eta}+\gamma}$ yields for (8) a fixed point equation

$$j_{\text{b}} = B(\gamma j_{\text{b}} + \delta\psi_{KL})\, e^{\eta_L} - B(-[\gamma j_{\text{b}} + \delta\psi_{KL}])\, e^{\eta_K} \tag{10}$$

for the non-dimensionalized edge current $j_{\text{b}} = j_n/j_0$. The right-hand side is a Scharfetter-Gummel expression where the argument of the Bernoulli function is shifted by γj_{b}. Hence, for $\gamma = 0$ the generalized flux j_{b} reduces to the classical Scharfetter-Gummel scheme (9) since the Blakemore function reduces to the Boltzmann function.

5 Solving for the generalized Scharfetter-Gummel flux numerically

For general distribution functions like (3) and (4), we cannot find closed expressions for the unknown current as a solution to (8). For this reason one may employ physically motivated approximate flux solutions. These *modified* Scharfetter-Gummel schemes we discuss in Section 6. To obtain more accurate flux approximations, we solve the generalized Scharfetter-Gummel scheme (8) numerically. The implementation is challgenging due to two reasons: First one needs to approximate the integral accurately and then solve a nonlinear equation. We use Gauss quadrature to approximate the integral. Not only is this highly efficient for smooth integrands but also the quadrature excludes the boundary nodes thus preventing the integrand from coming to close to a pole. [6] showed that no pole can appear within the integration limits. However, it might come very close to the domain of integration. Denoting

the integrand in (8) with $G(\eta; \delta\psi_{KL}, j)$ for $j = j_n/j_0$, we can approximate (8) by

$$H(j) := \sum_{i=1}^{N} w_i G(\eta_i; \delta\psi_{KL}, j) - 1 = 0, \tag{11}$$

where w_i are the integration weights and η_i the quadrature nodes.

We solve the nonlinear equation for the flux j via Newton's method, using the diffusion-enhanced Scharfetter-Gummel flux (13) as a starting guess. This choice is very crucial as already small perturbations may result in divergence. We treat pure drift and pure diffusive currents separately. For small drift and small diffusion we use the low-order series expansion of the unknonwn current derived by [3] to avoid numerical difficulties. In Figure 2, isosurfaces of the generalized Scharfetter-Gummel current using this method are shown for Fermi-Dirac and Gauss-Fermi statistics.

To verify the accuracy of our method, we tested how fast the current converges. We observed exponential convergence with respect to the number of quadrature nodes. For this quality assessment we used the Blakemore distribution function because in this case the solution to (8) can also be obtained via the fixed point equation (10). This analysis showed that usually $N = 16$ quadrature nodes are sufficient to resolve the integral equation (8) highly accurately.

6 Error analysis for modified Scharfetter-Gummel fluxes

Since solving an integral equation for each pair of neighboring discretization points $\mathbf{x}_K, \mathbf{x}_L$ appears to be too expensive in general, we present two modified schemes as approximate solutions to (8). They keep the beneficial Scharfetter-Gummel structure and are thermodynamically consistent. [3, 4] present more details and physical motivations.

6.1 Diffusion enhanced Scharfetter-Gummel scheme

[1, 10] suggest a logarithmic average of the diffusion enhancement $g(\eta) = \frac{1}{(\ln \mathcal{F}(\eta))'} = \mathcal{F}(\eta)/\mathcal{F}'(\eta) \geq 1$ given by

$$g_{KL} = \frac{\eta_L - \eta_K}{\log \mathcal{F}(\eta_L) - \log \mathcal{F}(\eta_K)}, \tag{12}$$

leading to the current approximation

$$j_{\mathsf{d}} = g_{KL} \left[B\left(\frac{\delta\psi_{KL}}{g_{KL}}\right) \mathcal{F}(\eta_L) - B\left(-\frac{\delta\psi_{KL}}{g_{KL}}\right) \mathcal{F}(\eta_K) \right]. \tag{13}$$

6.2 Inverse activity coefficients

In addition to the diffusion enhancement $g(\eta)$ another measure for the degeneracy is given by the inverse $\beta(\eta) = \mathcal{F}(\eta)/e^{\eta}$ of the activity coefficient, also known as degeneracy factor. For the Boltzmann distribution the factor $\beta(\eta)$ becomes one. For non-exponential distribution functions it is less than one. [5] derived the scheme

$$j_{\mathsf{a}} = -\bar{\beta}_{KL} \left(B(-\delta\psi_{KL})\, e^{\eta_K} - B(\delta\psi_{KL})\, e^{\eta_L} \right), \tag{14}$$

where $\bar{\beta}_{KL}$ denotes either an arithmetic or a geometric average between $\beta(\eta_K)$ and $\beta(\eta_L)$.

6.3 Error estimates and comparison

Finally, we compare the performance of both modified Scharfetter-Gummel schemes. For general distribution functions [3] derived error estimates between the modified fluxes ((13) and (14)) and the generalized Scharfetter-Gummel flux (8):

$$err_a(\bar{\eta}_{KL}, \delta\eta_{KL}, \delta\psi_{KL}) := |j_{\mathsf{a}} - j| \leq \frac{1}{2}\mathcal{F}(\bar{\eta}_{KL})|\delta\psi_{KL}\delta\eta_{KL}|, \tag{15}$$

$$err_d(\bar{\eta}_{KL}, \delta\eta_{KL}, \delta\psi_{KL}) := |j_{\mathsf{d}} - j| \leq \frac{1}{2}\frac{\mathcal{F}(\bar{\eta}_{KL})}{g(\bar{\eta}_{KL})}|\delta\psi_{KL}\delta\eta_{KL}|. \tag{16}$$

In these estimates $\bar{\eta}_{KL}$ denotes the arithmetic average

$$\bar{\eta}_{KL} := \frac{\eta_L + \eta_K}{2}$$

and higher order terms have been neglected. The bound for the diffusion-enhandced scheme (unlike for the inverse activity scheme) additionally depends on the inverse of the diffusion enhancement. Hence, if $g(\bar{\eta}_{KL})$ becomes large (strong degeneracy) the a priori error is considerably lower. [8] showed that high values of g can appear in devices operating at cryogenic temperatures.

Figure 3 depicts the errors in terms of $\delta\eta_{KL}$ and $\delta\psi_{KL}$ for fixed averages $\bar{\eta}_{KL}$ (guaranteeing a diffusion enhancement significantly larger than one) and different distribution functions. The errors vanish along the dashed lines indicating $\eta_K = \eta_L$ (pure drift current) as well as $\delta\psi_{KL} = \delta\eta_{KL}$ due to the consistency with the thermodynamic equilibrium. As predicted by the error estimates (15) and (16), the comparison in Figure 3 reveals that the error of diffusion-enhanced scheme (13) is considerably smaller than the error of the inverse activity scheme (14), in particular when the degeneracy becomes strong.

7 Conclusion

This paper extends previous error analysis for thermodynamically consistent fluxes by [3]. The authors focussed on general analytical results illustrating them using the Blakemore distribution function. The authors showed that the diffusion-enhanced scheme is superior to the inverse activities scheme when the diffusion enhancement is large, i. e. degeneracy effects are strong. In the present paper, we confirm that this holds true for a larger class of distribution functions, in particular the Fermi-Dirac integral of order 1/2, the Gauss-Fermi integral and the degenerate limit $\mathcal{F}(\eta) = \frac{2}{\sqrt{\pi}}\eta^{3/2}$ which becomes important at cryogenic temperatures.

The comparison is based on studying the difference between modified fluxes and the more accurate generalized Scharfetter-Gummel flux. To obtain the generalized flux, we had to numerically solve an integral equation. For this reason, we devised an algorithm based on Gauss quadrature and Newton's method. The exponential convergence with respect to the number of quadrature nodes makes the numerical implementation of the generalized flux an interesting alternative to the existing modified Scharfetter-Gummel schemes.

[3] analyzed the beneficial influence of the diffusion-enhanced flux on the solution of the fully coupled van Roosbroeck system via a p-i-n benchmark. This simulation was restricted to the Blakemore distribution function. However, since the error plots in Figure 3 for the Fermi-Dirac and Gauss-Fermi distribution function as well as the degenerate limit are comparable, it is reasonable to expect similar performance gains for the fully coupled van Roosbroeck system.

(a) Fermi-Dirac integral $F_{1/2}$, $\bar{\eta}_{KL} = 5$: Diffusion enhancement $g(5) \approx 3.58$

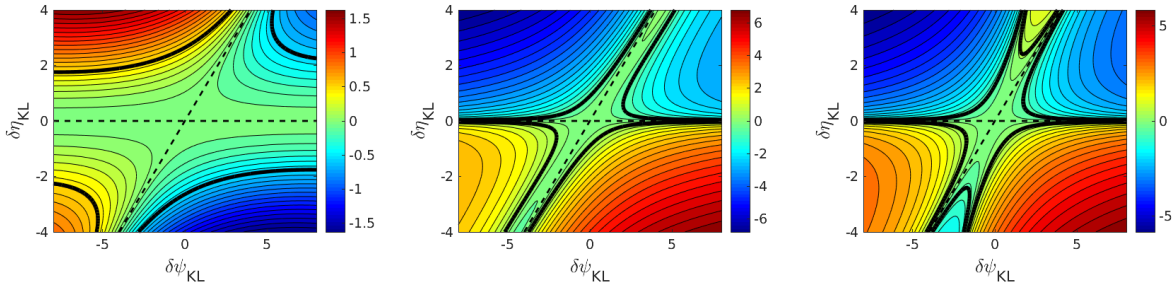

(b) Degenerate limit $\frac{2}{\sqrt{\pi}}\eta^{3/2}$, $\bar{\eta}_{KL} = 60$: Diffusion enhancement $g(60) = 40$

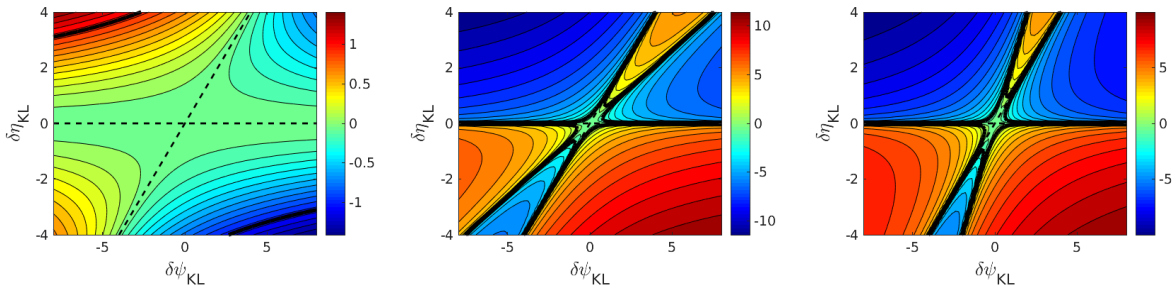

(c) Gauss-Fermi $\mathcal{G}(\eta; \sigma = 5)$, $\bar{\eta}_{KL} = -15$: Diffusion enhancement $g(-15) \approx 1.74$

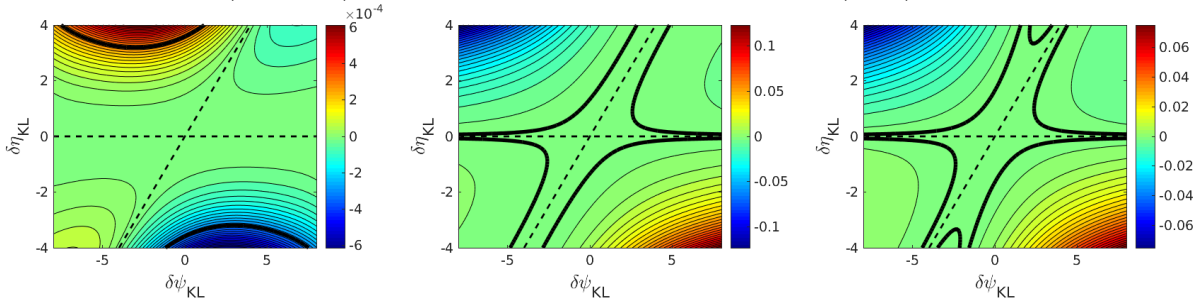

(d) Gauss-Fermi $\mathcal{G}(\eta; \sigma = 5)$, $\bar{\eta}_{KL} = 0$: Diffusion enhancement $g(0) \approx 6.66$

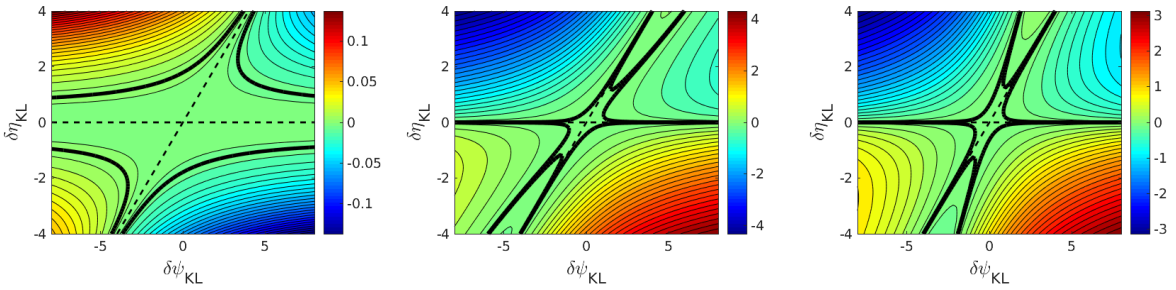

Figure 3: Logarithmic absolute errors between the generalized Scharfetter-Gummel and modified schemes depending on the potential differences $\delta\psi_{KL}$ and $\delta\eta_{KL}$ for a fixed value of $\bar{\eta}_{KL}$, cp. (15) and (16). Each row corresponds to a different distribution function and each column correponds to a different flux approximation: diffusion enhanced scheme (left), the arithmetically averaged inverse activity scheme (middle) and the geometrically averaged one (right). The dashed lines show where generalized and modified schemes agree exactly. The bold black lines highlight the same contour level in each row.

Acknowledgements

This work received funding via the Research Center Matheon supported by ECMath in project D-CH11 and the DFG CRC 787 “Semiconductor Nanophotonics”.

References

[1] Bessemoulin-Chatard, M.: A finite volume scheme for convection–diffusion equations with nonlinear diffusion derived from the Scharfetter–Gummel scheme. Numerische Mathematik **121**(4), 637–670 (2012). DOI 10.1007/s00211-012-0448-x

[2] Eymard, R., Fuhrmann, J., Gärtner, K.: A finite volume scheme for nonlinear parabolic equations derived from one-dimensional local Dirichlet problems. Numer. Math. **102**(3), 463–495 (2006)

[3] Farrell, P., Koprucki, T., Fuhrmann, J.: Computational and analytical comparison of flux discretizations for the semiconductor device equations beyond boltzmann statistics. Journal of Computational Physics **346**, 497 – 513 (2017). DOI https://doi.org/10.1016/j.jcp.2017.06.023

[4] Farrell, P., Rotundo, N., Doan, D.H., Kantner, M., Fuhrmann, J., Koprucki, T.: Mathematical methods: Drift-diffusion models. In: J. Piprek (ed.) Handbook of Optoelectronic Device Modeling and Simulation, chap. 50, pp. 733–772. Taylor & Francis (2017)

[5] Fuhrmann, J.: Comparison and numerical treatment of generalised Nernst-Planck models. Comp. Phys. Comm. **196**, 166 – 178 (2015). DOI http://dx.doi.org/10.1016/j.cpc.2015.06.004

[6] Gärtner, K.: Existence of bounded discrete steady state solutions of the van Roosbroeck system with monotone Fermi–Dirac statistic functions. Journal of Computational Electronics **14**(3), 773–787 (2015). DOI 10.1007/s10825-015-0712-2

[7] Jüngel, A.: Numerical approximation of a drift-diffusion model for semiconductors with nonlinear diffusion. ZAMM **75**(10), 783–799 (1995)

[8] Kantner, M., Koprucki, T.: Numerical simulation of carrier transport in semiconductor devices at cryogenic temperatures. Opt. Quant. Electronics **48**(12), 1–7 (2016). DOI 10.1007/s11082-016-0817-2

[9] Koprucki, T., Gärtner, K.: Discretization scheme for drift-diffusion equations with strong diffusion enhancement. Opt. Quant. Electronics **45**(7), 791–796 (2013). DOI 10.1007/s11082-013-9673-5

[10] Koprucki, T., Rotundo, N., Farrell, P., Doan, D.H., Fuhrmann, J.: On thermodynamic consistency of a Scharfetter–Gummel scheme based on a modified thermal voltage for drift-diffusion equations with diffusion enhancement. Optical and Quantum Electronics **47**(6), 1327–1332 (2015). DOI 10.1007/s11082-014-0050-9

[11] Paasch, G., Scheinert, S.: Charge carrier density of organics with Gaussian density of states: Analytical approximation for the Gauss-Fermi integral. J. Appl. Phys. **107**(10), 104,501 (2010). DOI DOI:10.1063/1.3374475. URL http://dx.doi.org/doi/10.1063/1.3374475

[12] Purbo, O.W., Cassidy, D.T., Chisholm, S.H.: Numerical model for degenerate and heterostructure semiconductor devices. Journal of Applied Physics **66**(10), 5078–5082 (1989)

[13] Scharfetter, D., Gummel, H.: Large-signal analysis of a silicon Read diode oscillator. IEEE Trans. Electr. Dev. **16**(1), 64–77 (1969). DOI 10.1109/T-ED.1969.16566

[14] Stodtmann, S., Lee, R.M., Weiler, C.K.F., Badinski, A.: Numerical simulation of organic semiconductor devices with high carrier densities. Journal of Applied Physics **112**(11) (2012). DOI http://dx.doi.org/10.1063/1.4768710